Electronic Supplementary Information (ESI) for New Journal of Chemistry

Hydroxynicotinic acids crystallisation and solubility systematic studies

Catarina V. Esteves*

Centro de Química Estrutural, Institute of Molecular Sciences, Faculdade de Ciências,

Universidade de Lisboa, 1749-016 Lisboa, Portugal

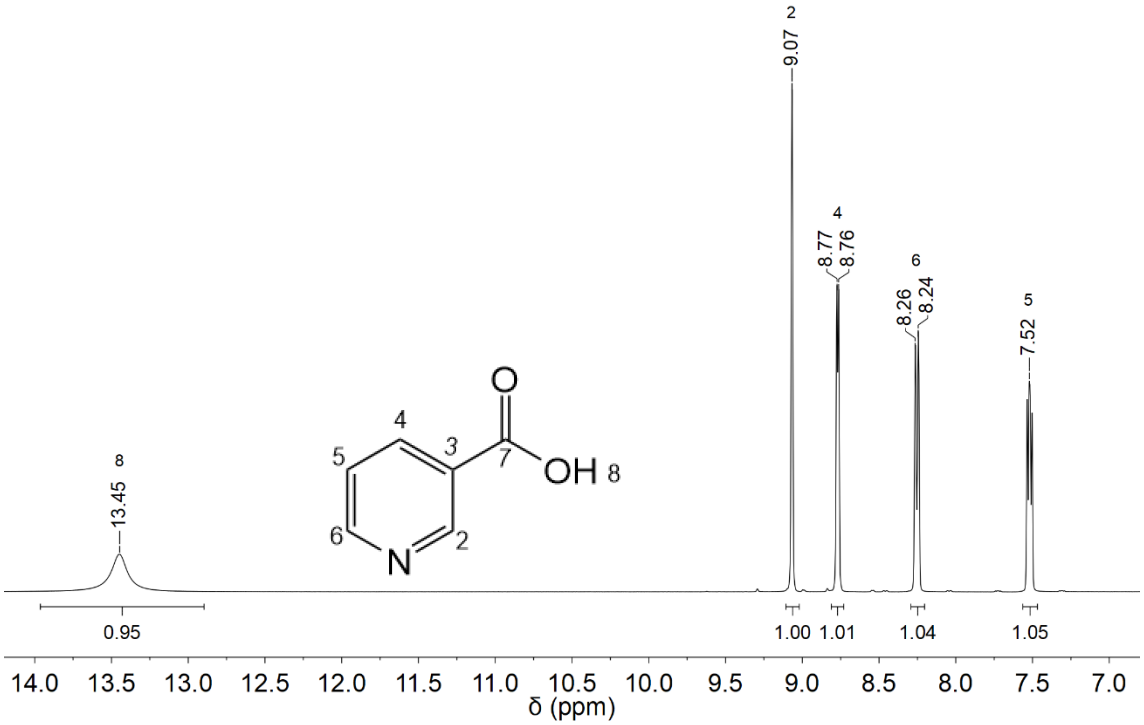

Fig. S1. ^{1}H NMR spectrum of NA in DMSO-d_6.

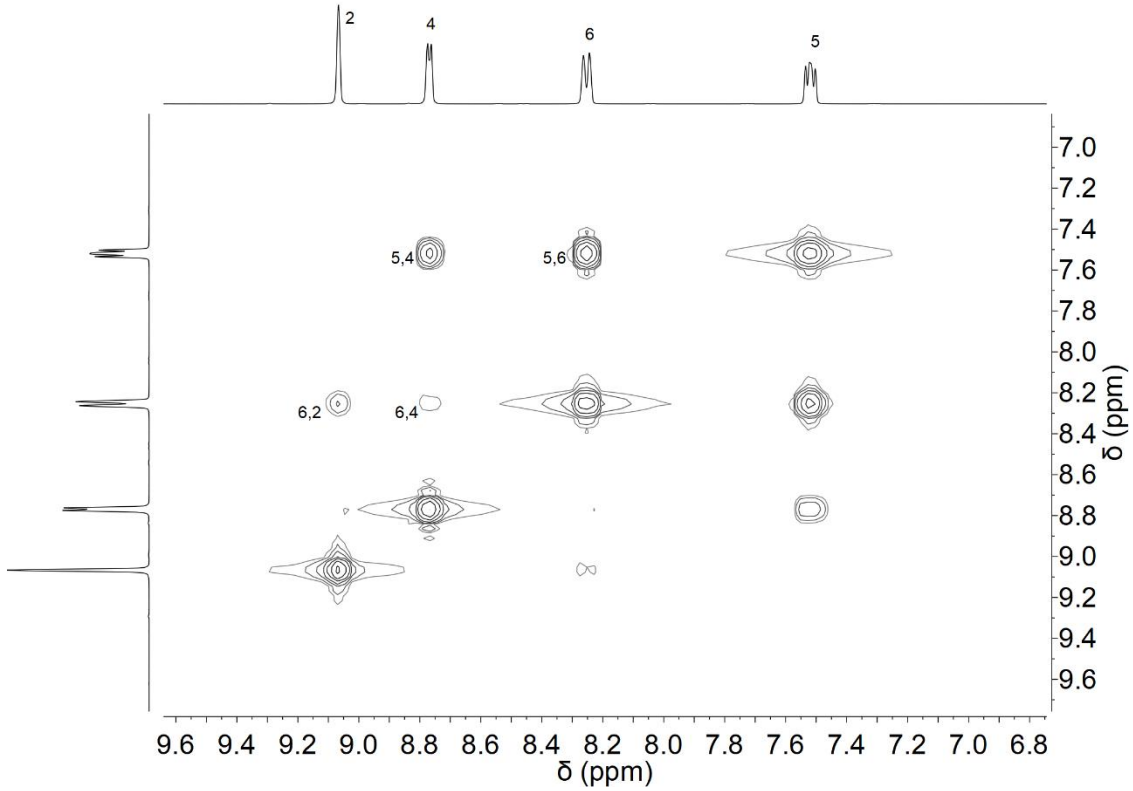

Fig. S2. COSY spectrum of NA in DMSO-d_6.

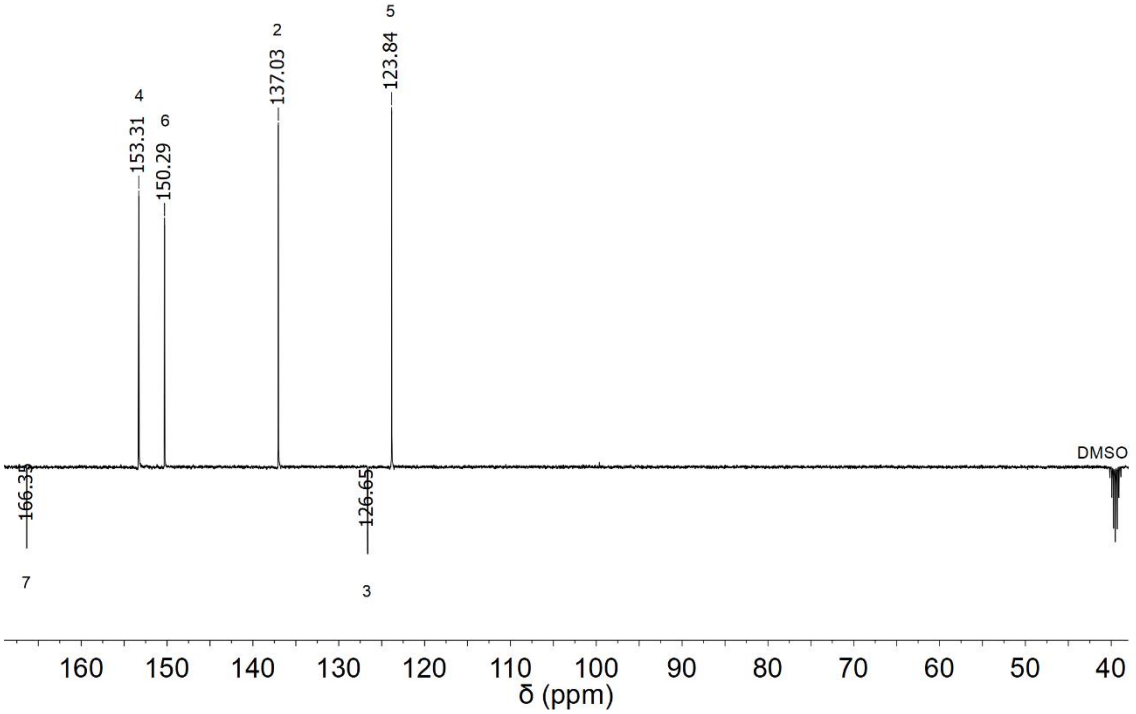

Fig. S3. ^{13}C-APT spectrum of NA in DMSO-d_6.

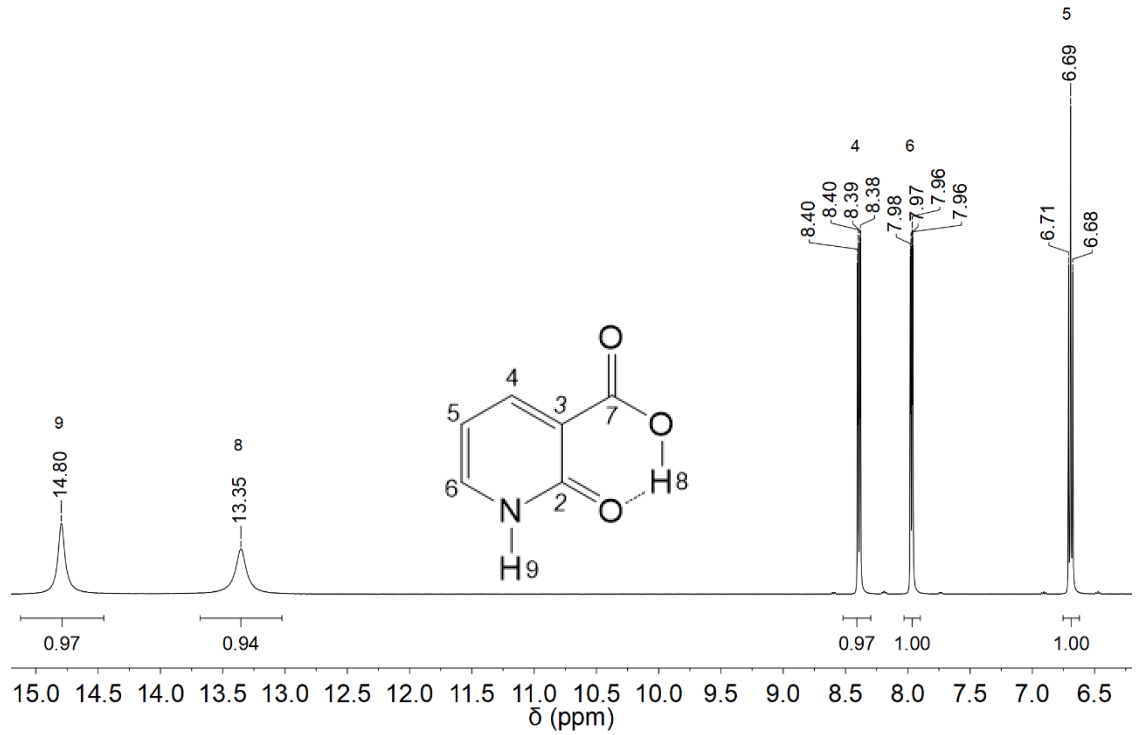

Fig. S4. ^{1}H NMR spectrum of 2HNA in DMSO-d_6.

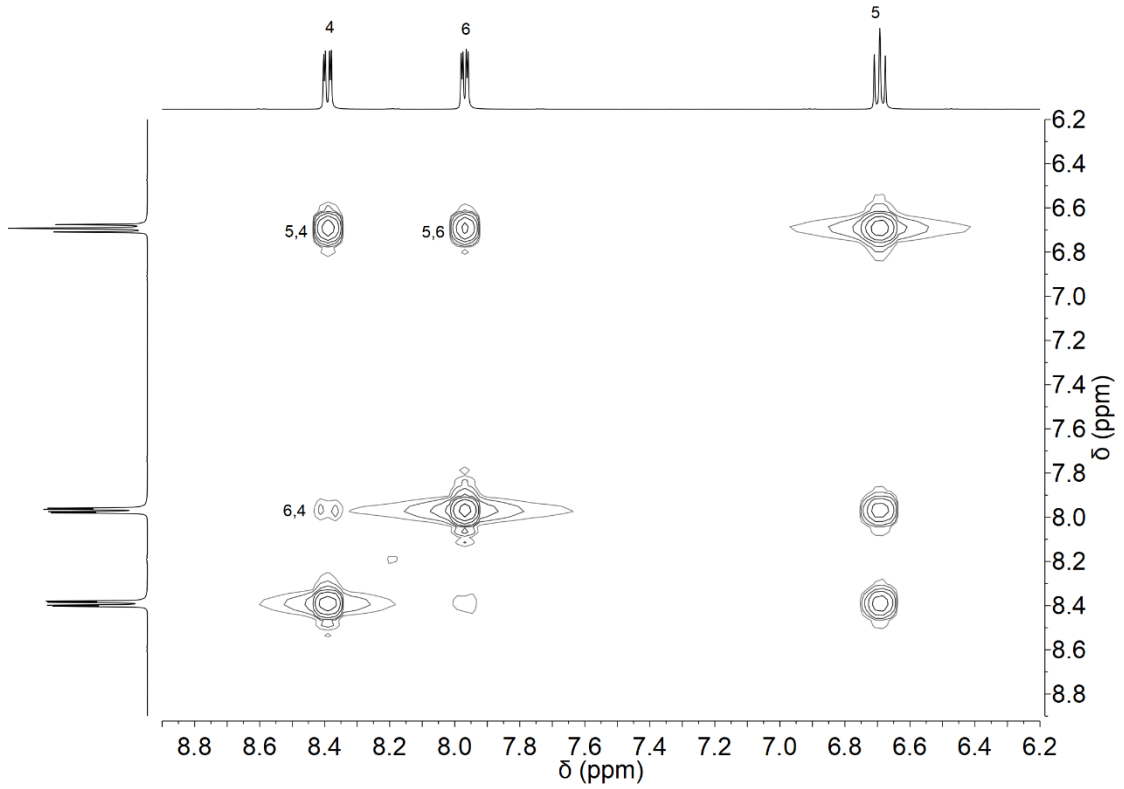

Fig. S5. COSY spectrum of 2HNA in DMSO-d_6.

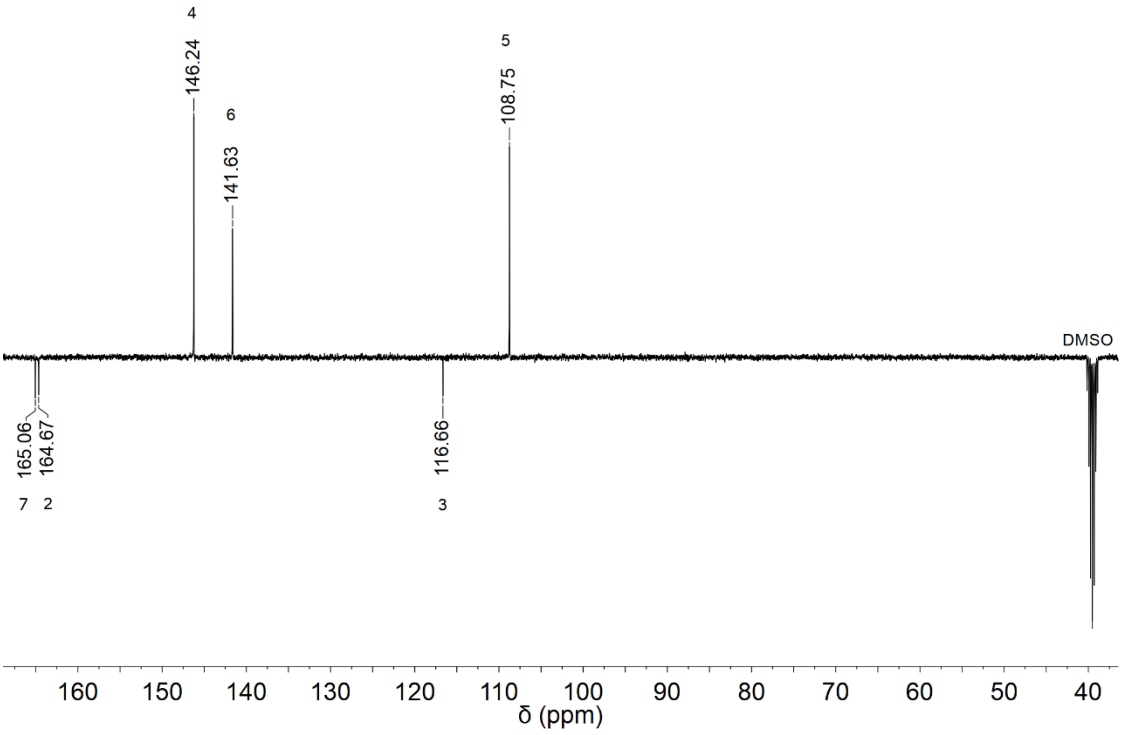

Fig. S6. ^{13}C-APT spectrum of 2HNA in DMSO-d_6.

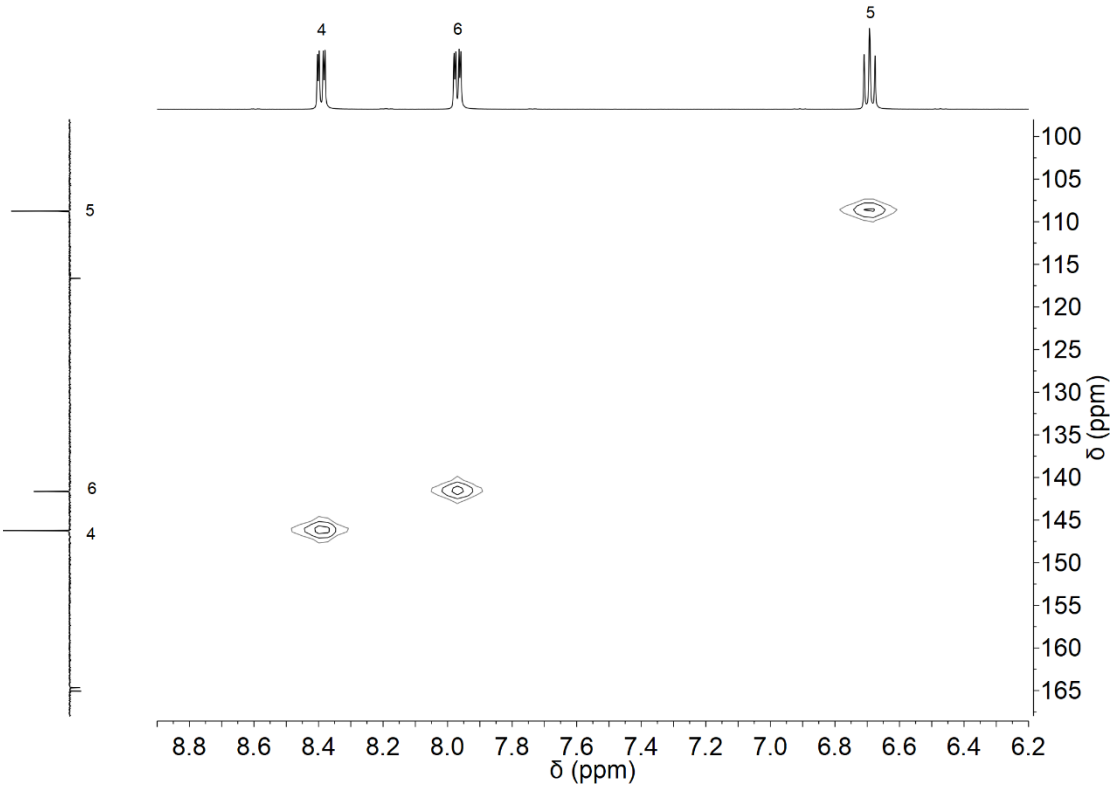

Fig. S7. HMQC spectrum of 2HNA in DMSO-d_6.

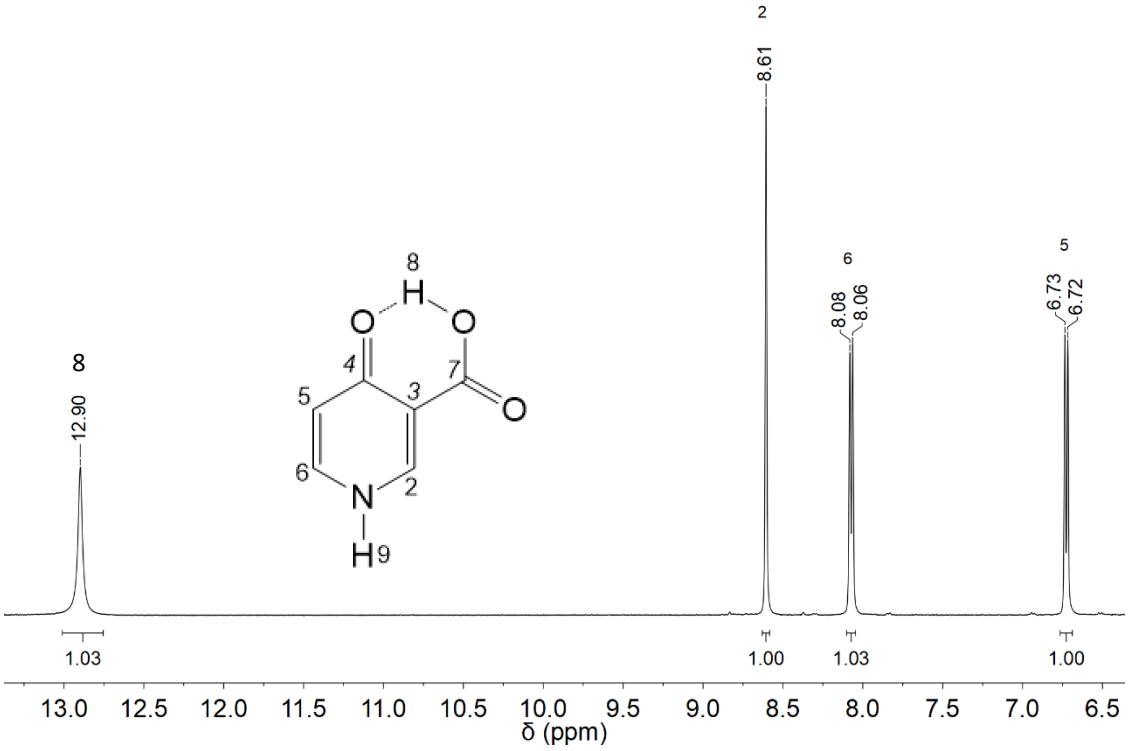

Fig. S8. ^{1}H NMR spectrum of 4HNA in DMSO-d_6.

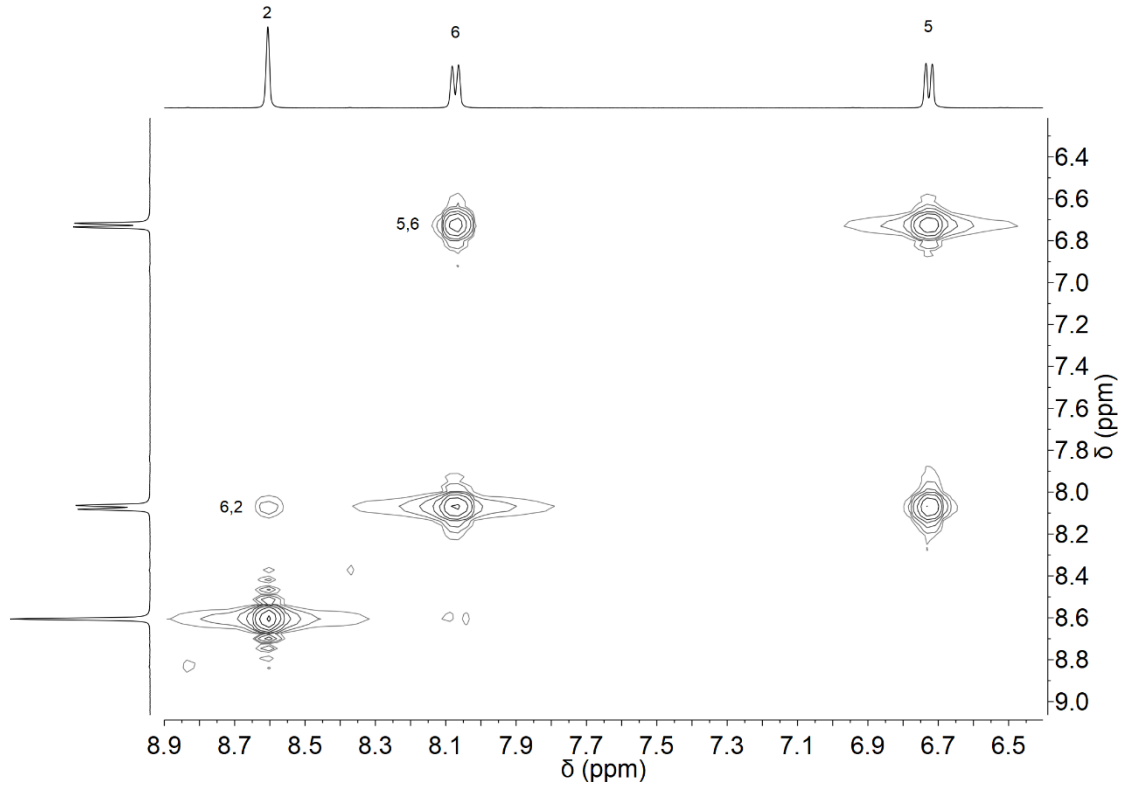

Fig. S9. COSY spectrum of 4HNA in DMSO-d_6.

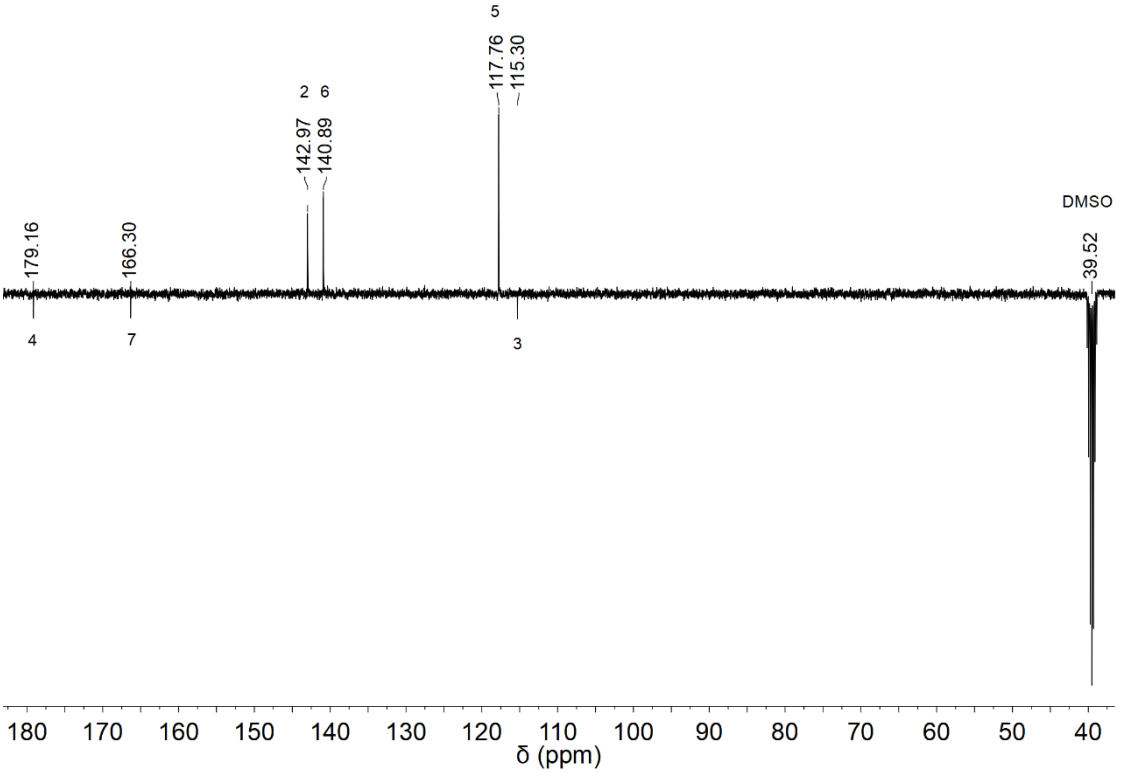

Fig. S10. ^{13}C-APT spectrum of 4HNA in DMSO-d_6.

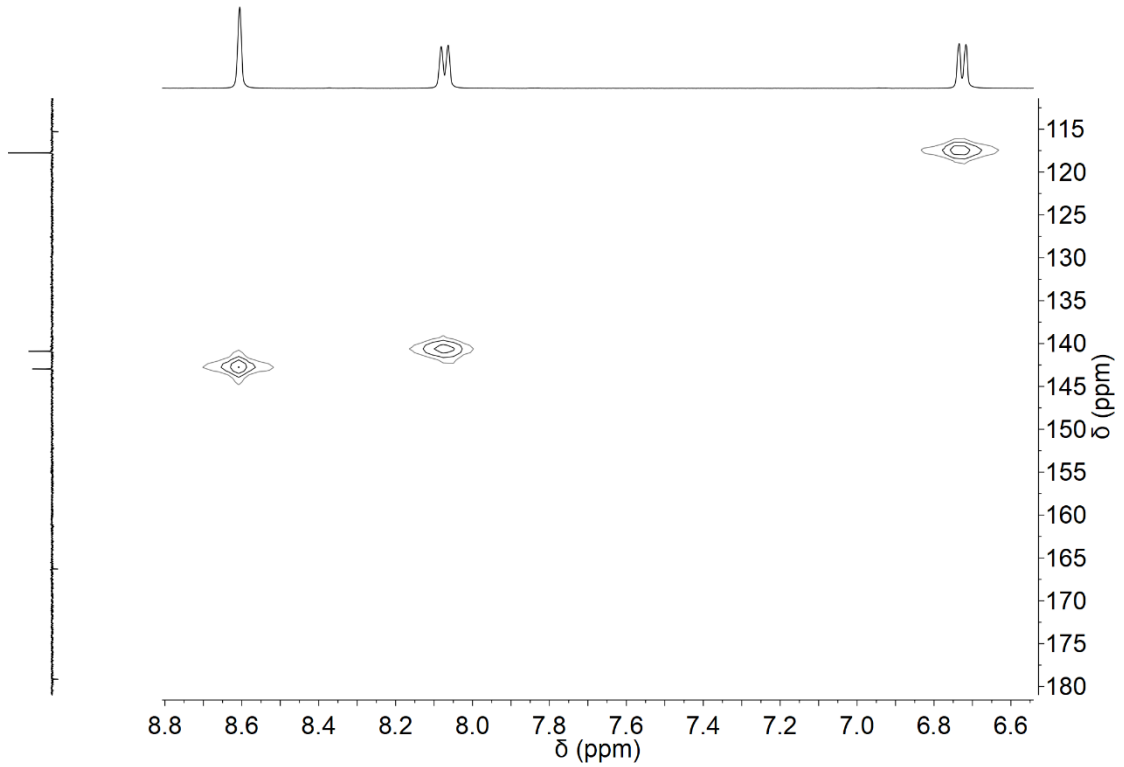

Fig. S11. HMQC spectrum of 4HNA in DMSO-d_6.

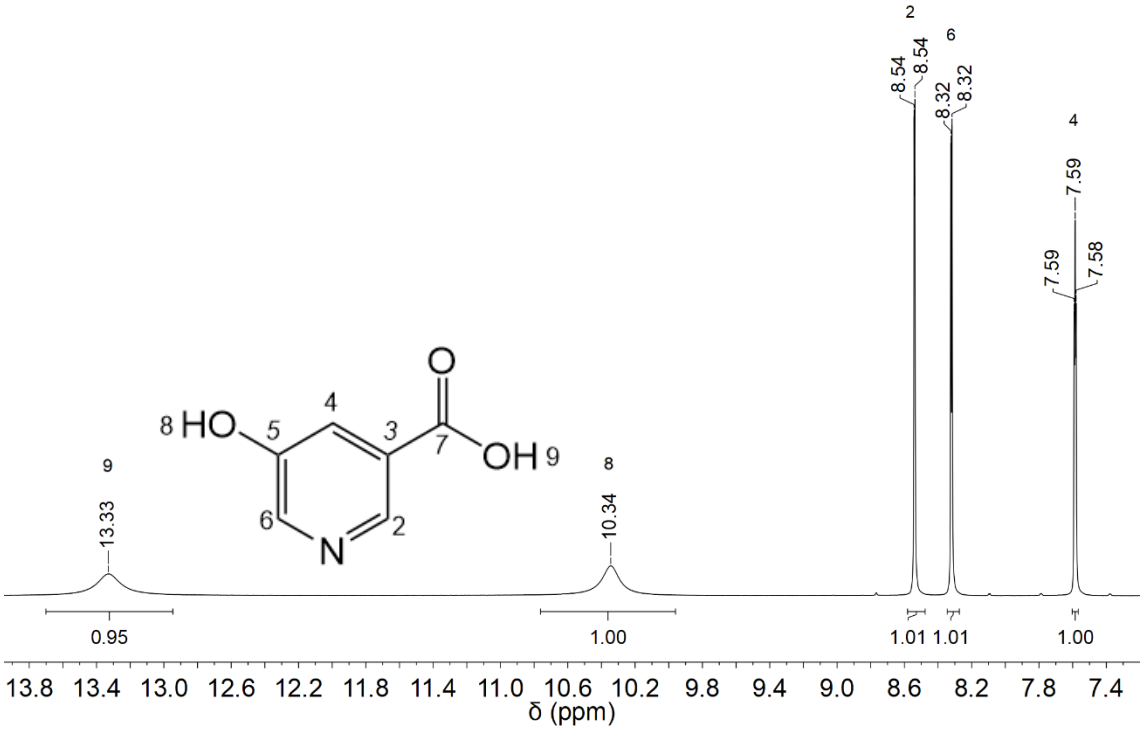

Fig. S12. ^{1}H NMR spectrum of 5HNA in DMSO-d_6.

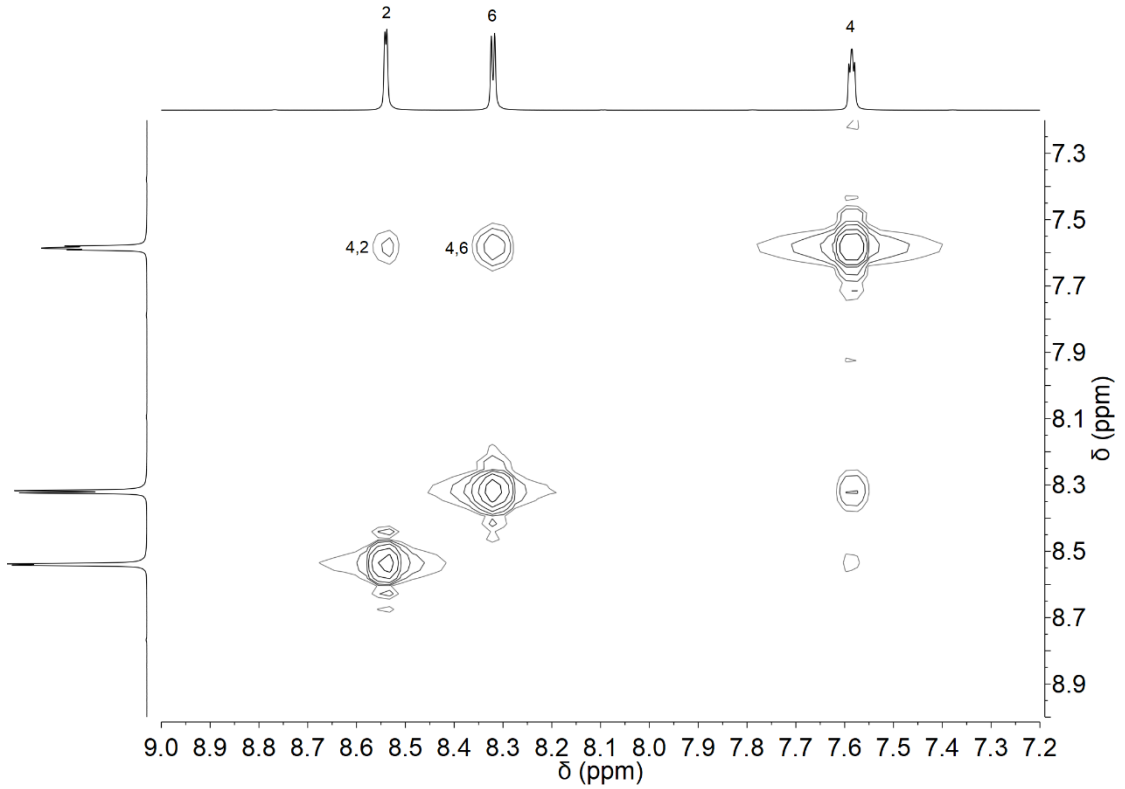

Fig. S13. COSY spectrum of 5HNA in DMSO-d_6.

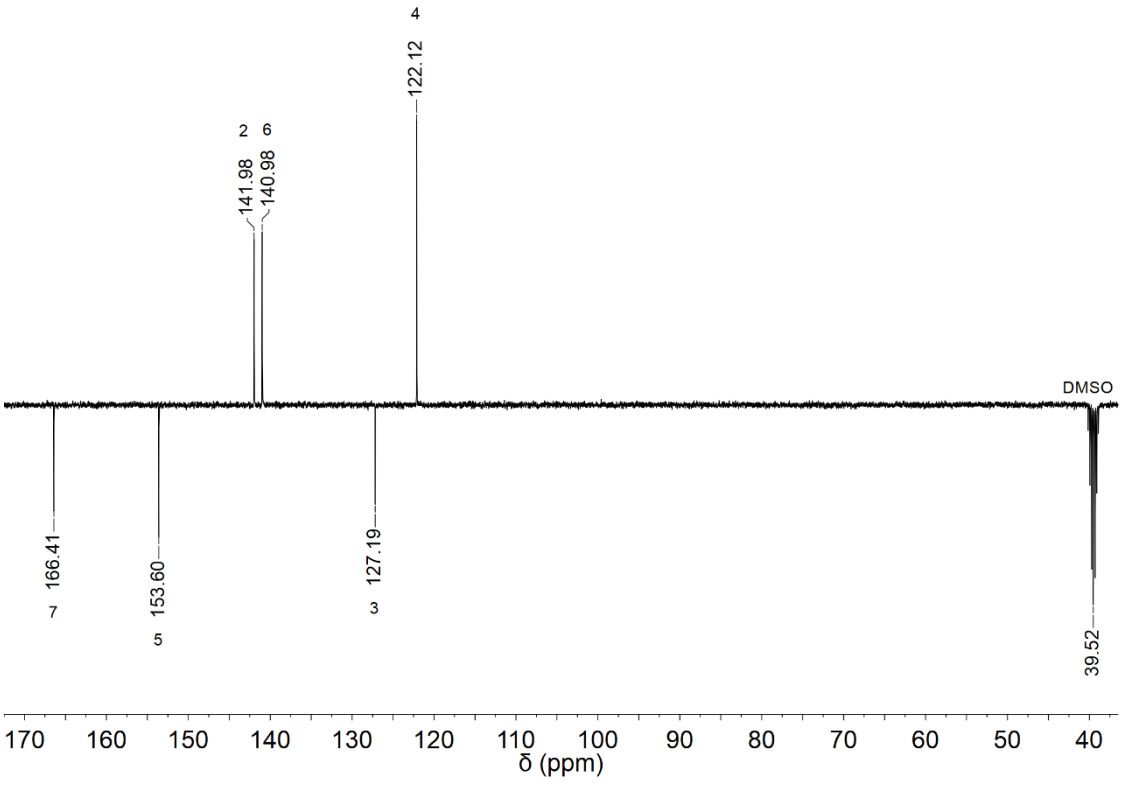

Fig. S14. ^{13}C-APT spectrum of 5HNA in DMSO-d_6.

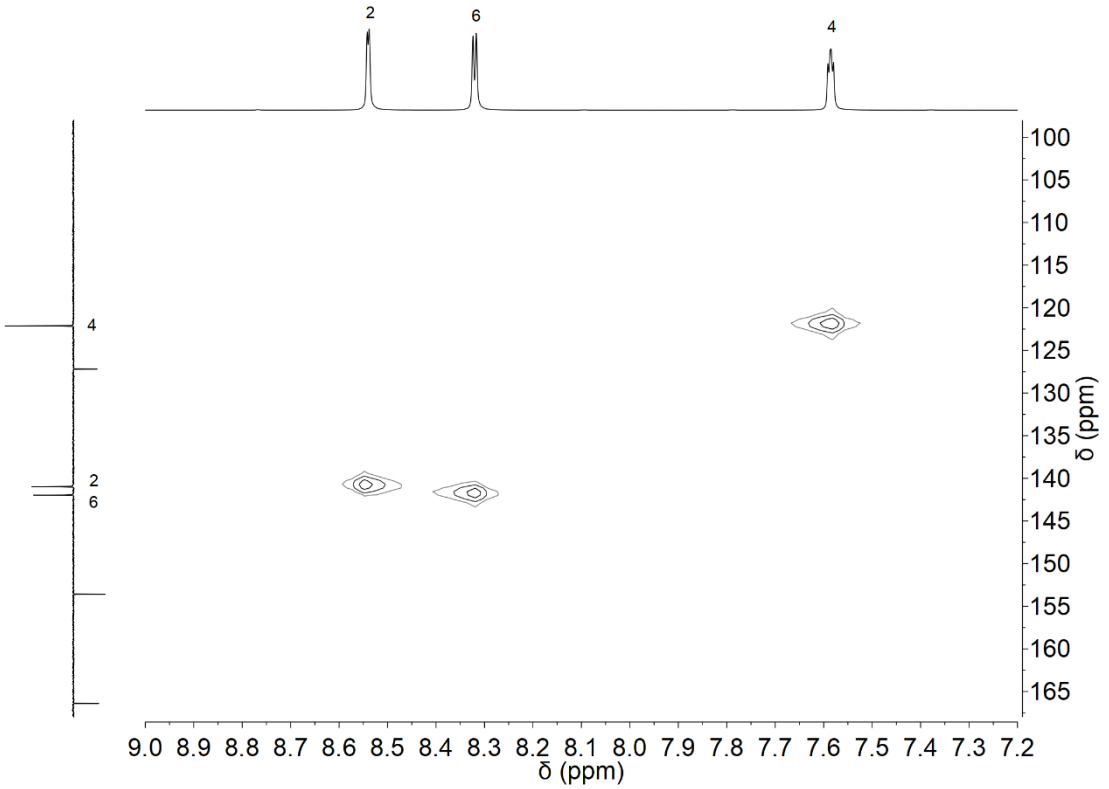

Fig. S15. HMQC spectrum of 5HNA in DMSO-d_6.

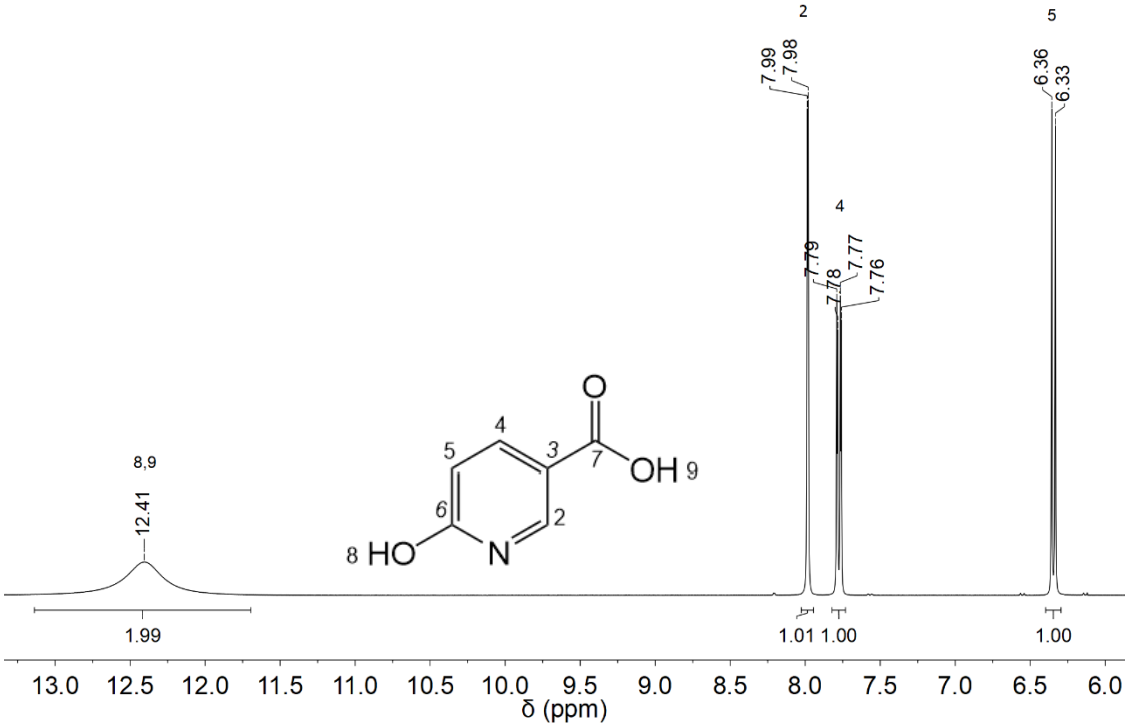

Fig. S16. ^{1}H NMR spectrum of 6HNA in DMSO-d_6.

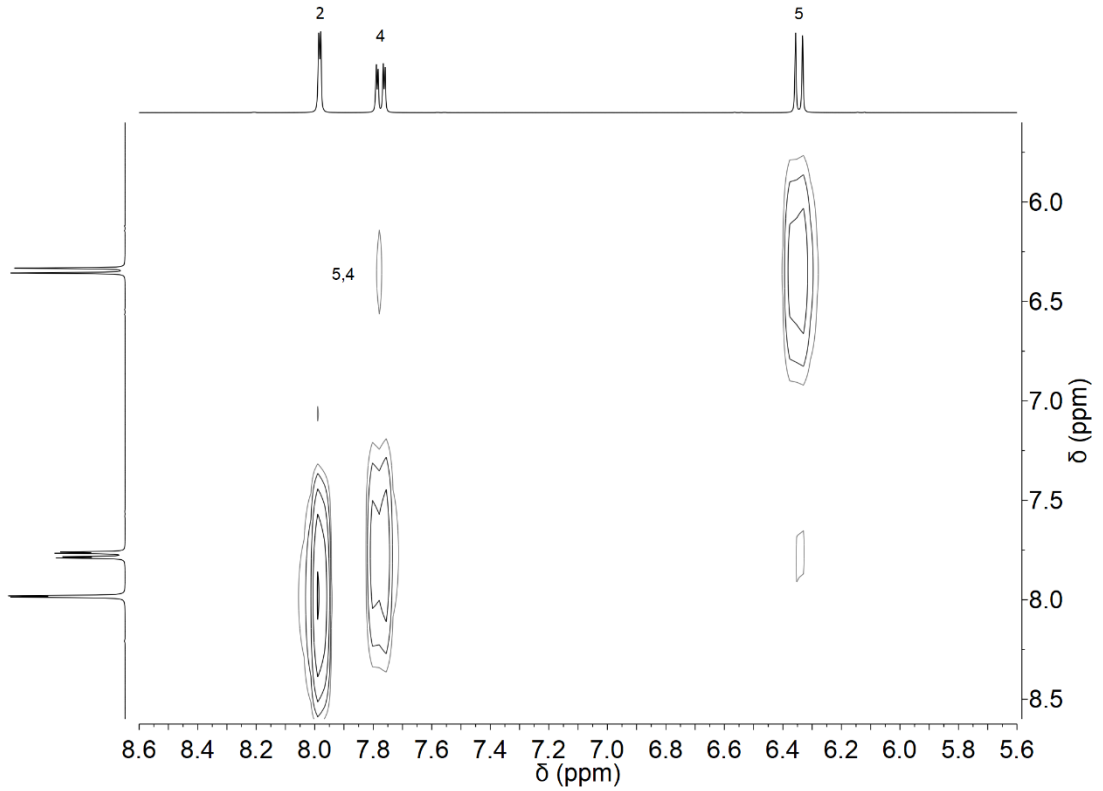

Fig. S17. COSY spectrum of 6HNA in DMSO-d_6.

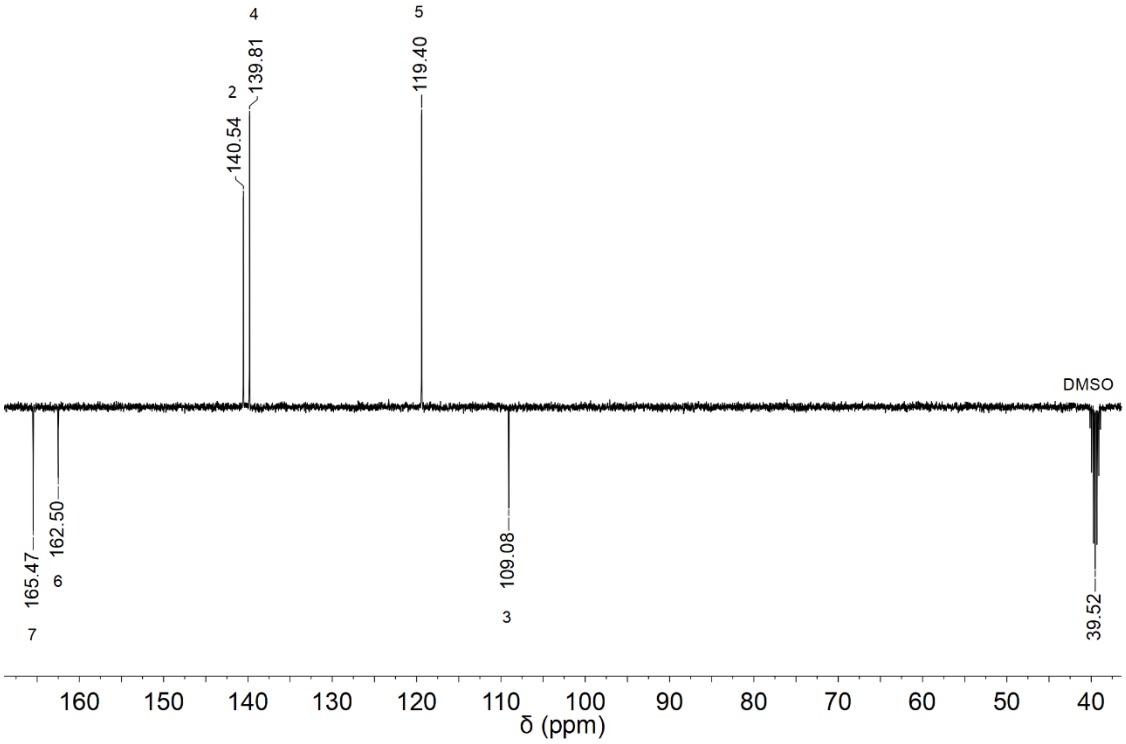

Fig. S18. ^{13}C-APT spectrum of 6HNA in DMSO-d_6.

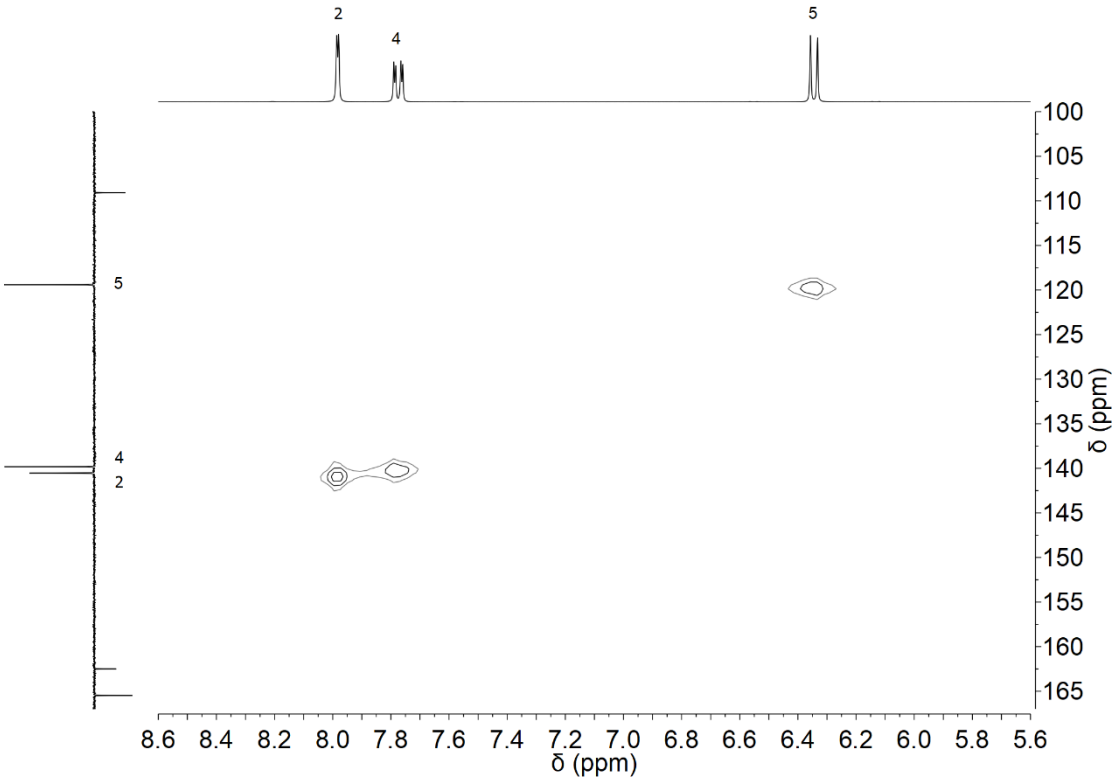

Fig. S19. HMQC spectrum of 6HNA in DMSO-d_6.

Table S1

Assignment of the ^{1}H and ^{13}C spectra of 2-, 4-, 5-, and 6-hydroxynicotinic acids at 293±2 K in DMSO-d_6.

	NA			**2HNA**			**4HNA**			**5HNA**			**6HNA**	
Type	*m*	^{1}H (ppm)	^{13}C (ppm)	*m*	^{1}H (ppm)	^{13}C (ppm)	*m*	^{1}H (ppm)	^{13}C (ppm)	*m*	^{1}H (ppm)	^{13}C (ppm)	*m*	^{1}H (ppm)	^{13}C (ppm)
$C_{Py}OH$						164.67			179.16			153.60			162.50
$C_{Py}COOH$			126.65			116.66			115.30			127.19			109.08
$CH_{Py\ Position\ 2}$	*s*	9.07	137.03												
$CH_{Py\ Position\ 4}$	*d*	8.77-8.76	153.31	*dd*	8.40-8.38	164.24	*s*	8.61	142.97	*d*	8.54	141.98	*d*	7.99-7.98	140.54
$CH_{Py\ Position\ 5}$	*dt*	7.53-7.50	123.84	*t*	6.71-6.88	108.75	*d*	6.73-6.72	117.76	*t*	7.59-7.58	122.12	*dd*	7.79-7.76	139.81
$CH_{Py\ Position\ 6}$	*dd*	8.26-8.24	150.29	*dd*	7.98-7.96	141.63	*d*	8.06	140.89	*d*	8.32	140.98	*d*	6.36	119.40
C═O			166.35			165.06			166.30			166.41			165.47
$OH_{carboxylic\ acid}$	*bs*	13.45		*bs*	13.35		*bs*	12.90		*bs*	13.33		*bs*	12.41	
$OH_{hydroxyl\ group}$				*bs*			*bs*			*bs*	10.34		*bs*	12.41	
NH				*bs*	14.80										

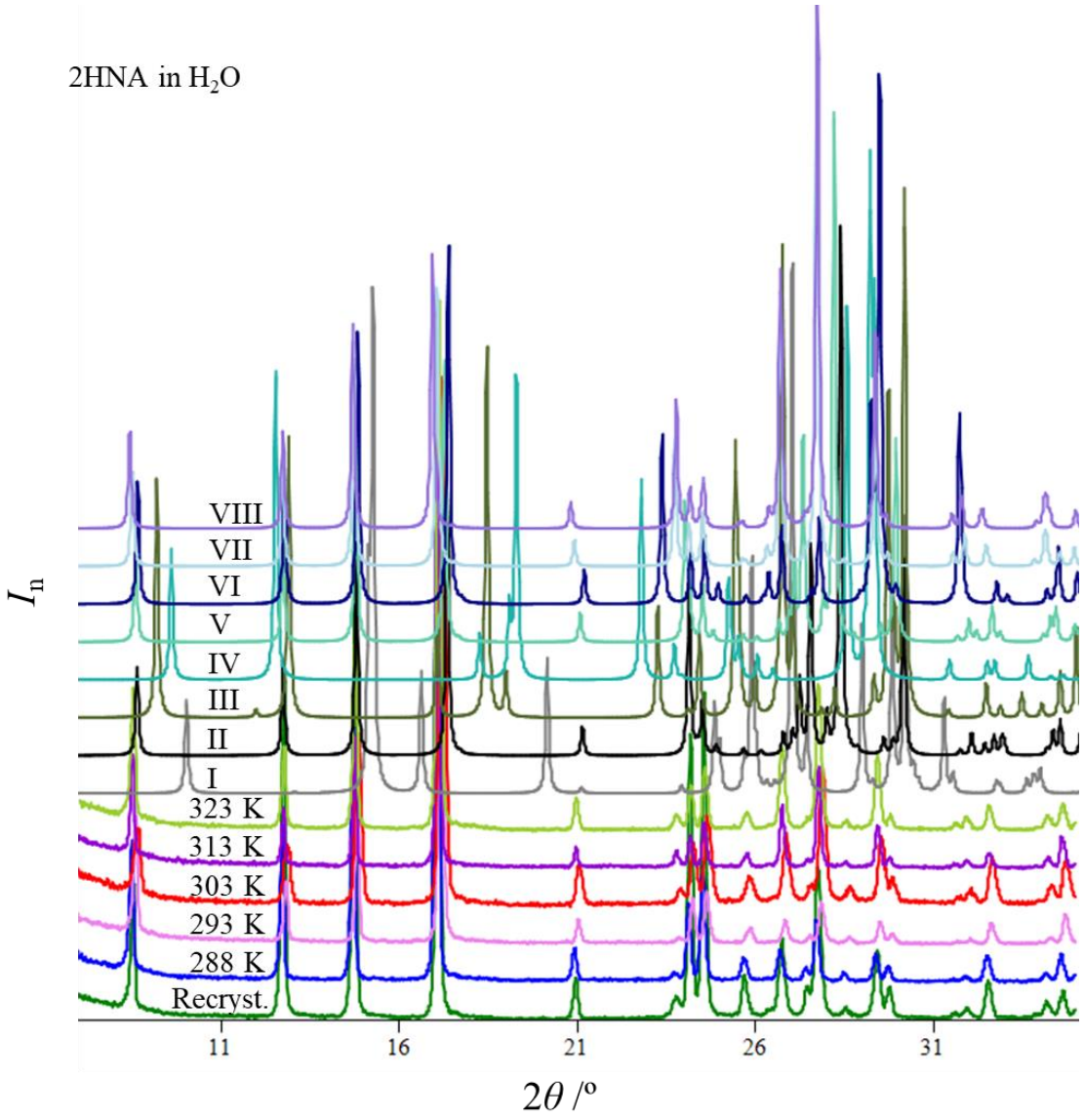

Fig. S20. Comparison of X-ray diffraction patterns obtained at room temperature for the recrystallized 2HNA (bottom), the powders obtained during the solubility experiment performed in H_2O (middle patterns matching form VIII, the stabilization temperatures used in the slurry in equilibrium with the saturated solution are specified), and the patterns from the literature polymorph structures (top, for references see Table 2 in the manuscript). All the diffractograms were normalized to the peak of highest intensity (I_n) and plotted using EasyGraphII [1].

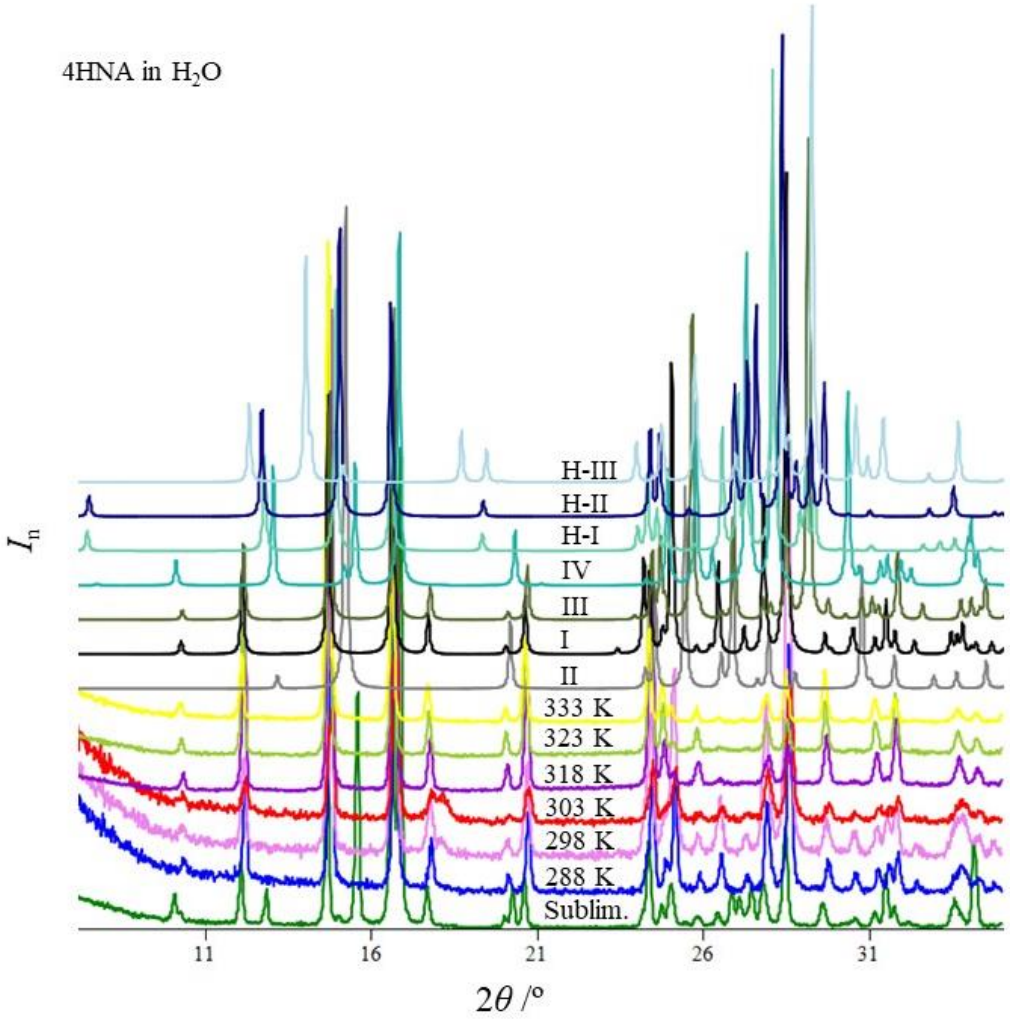

Fig. S21. Comparison of X-ray diffraction patterns obtained at room temperature for the sublimed 4HNA (bottom), the powders obtained during the solubility experiment performed in H_2O (middle patterns matching form I, the stabilization temperatures used in the slurry in equilibrium with the saturated solution are specified), and the patterns from the literature polymorph and hydrate structures (top, for references see Table 2). All the diffractograms were normalized to the peak of highest intensity (I_n) and plotted using EasyGraphII [1].

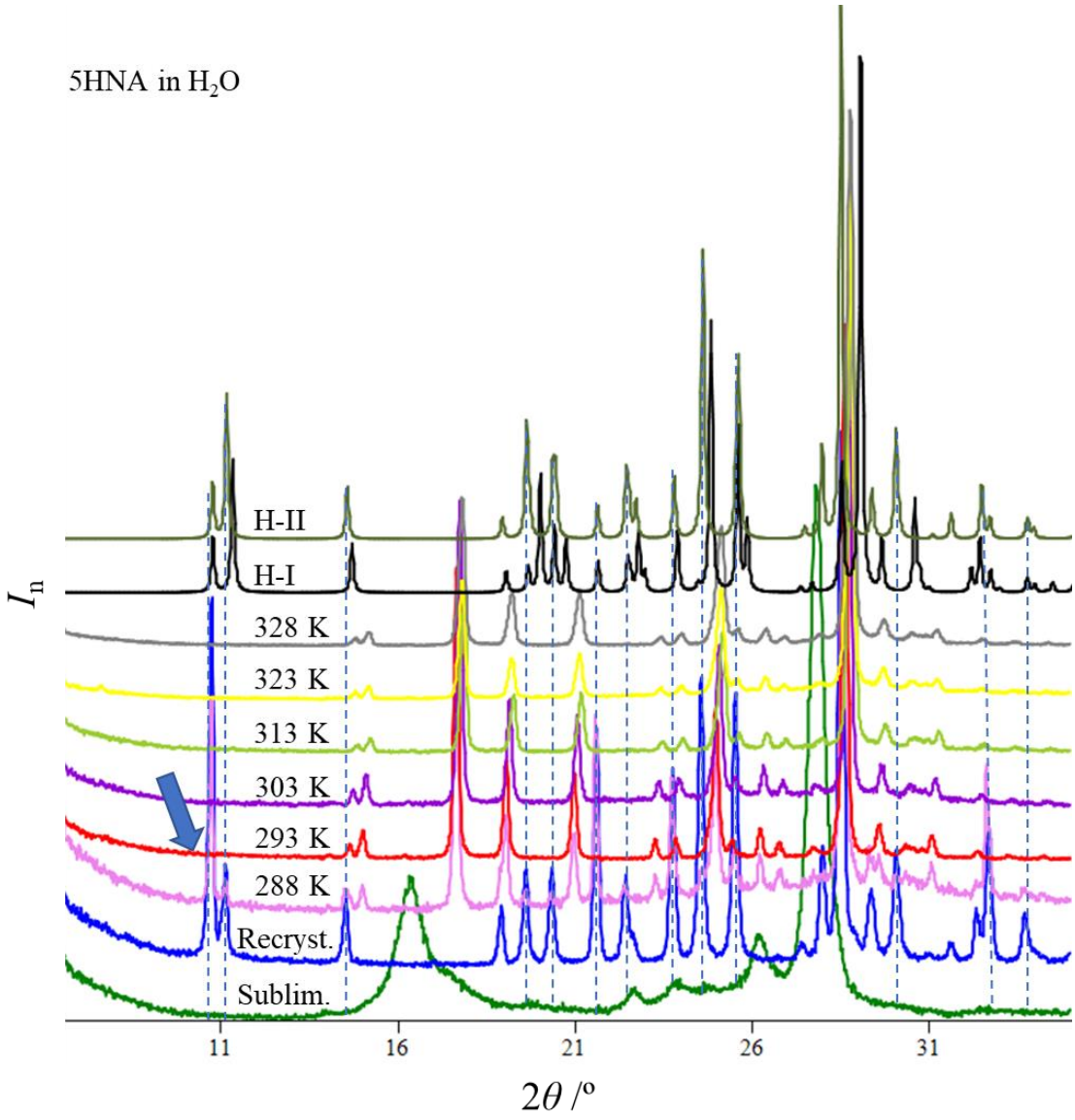

Fig. S22. Comparison of X-ray diffraction patterns obtained at room temperature for both sublimed and recrystallized 5HNA, bottom pattern, the powders obtained during the solubility experiment performed in H_2O, middle patterns, the stabilization temperatures used in the slurry in equilibrium with the saturated solution are specified, and the patterns from the hydrate from the literature [2] (top). All the diffractograms were normalized to the peak of highest intensity (I_n) and plotted using EasyGraphII [1].

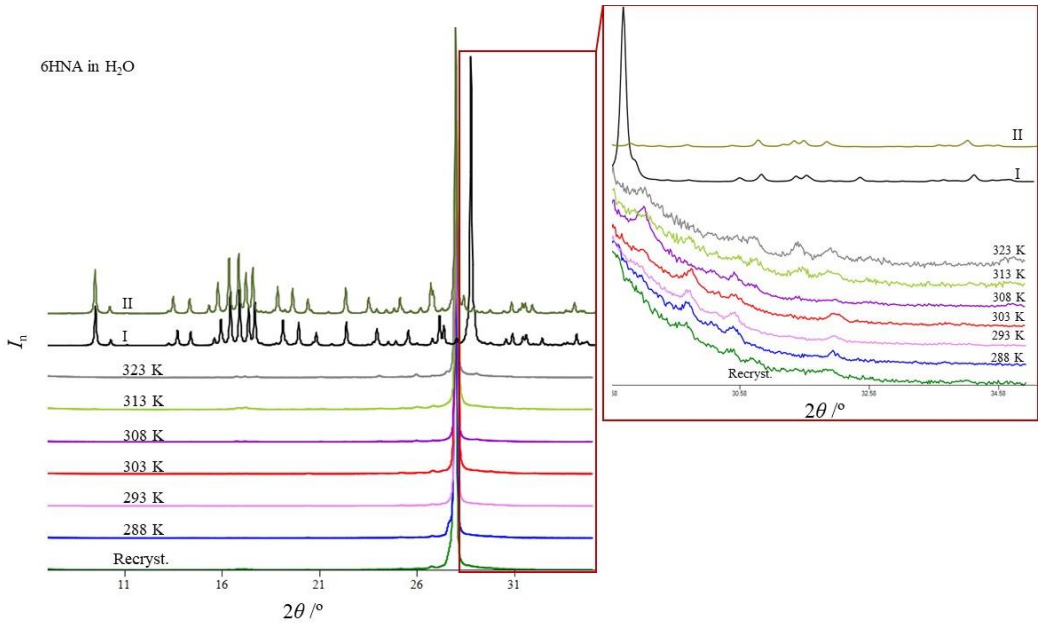

Fig. S23. Comparison of X-ray diffraction patterns obtained at room temperature for the recrystallized 6HNA (bottom), the powders obtained during the solubility experiment performed in H_2O (middle patterns matching form II, the stabilization temperatures used in the slurry in equilibrium with the saturated solution are specified), and the patterns from the literature polymorph structures (top, for references see Table 1). A zoom was added focusing on the region above the observed preferential orientation (2θ = 28.0) to ensure that at 2θ = 28.8 no peak was found, corroborating that the patterns obtained were in form II. All the diffractograms were normalized to the peak of highest intensity (I_n) and plotted using EasyGraphII [1].

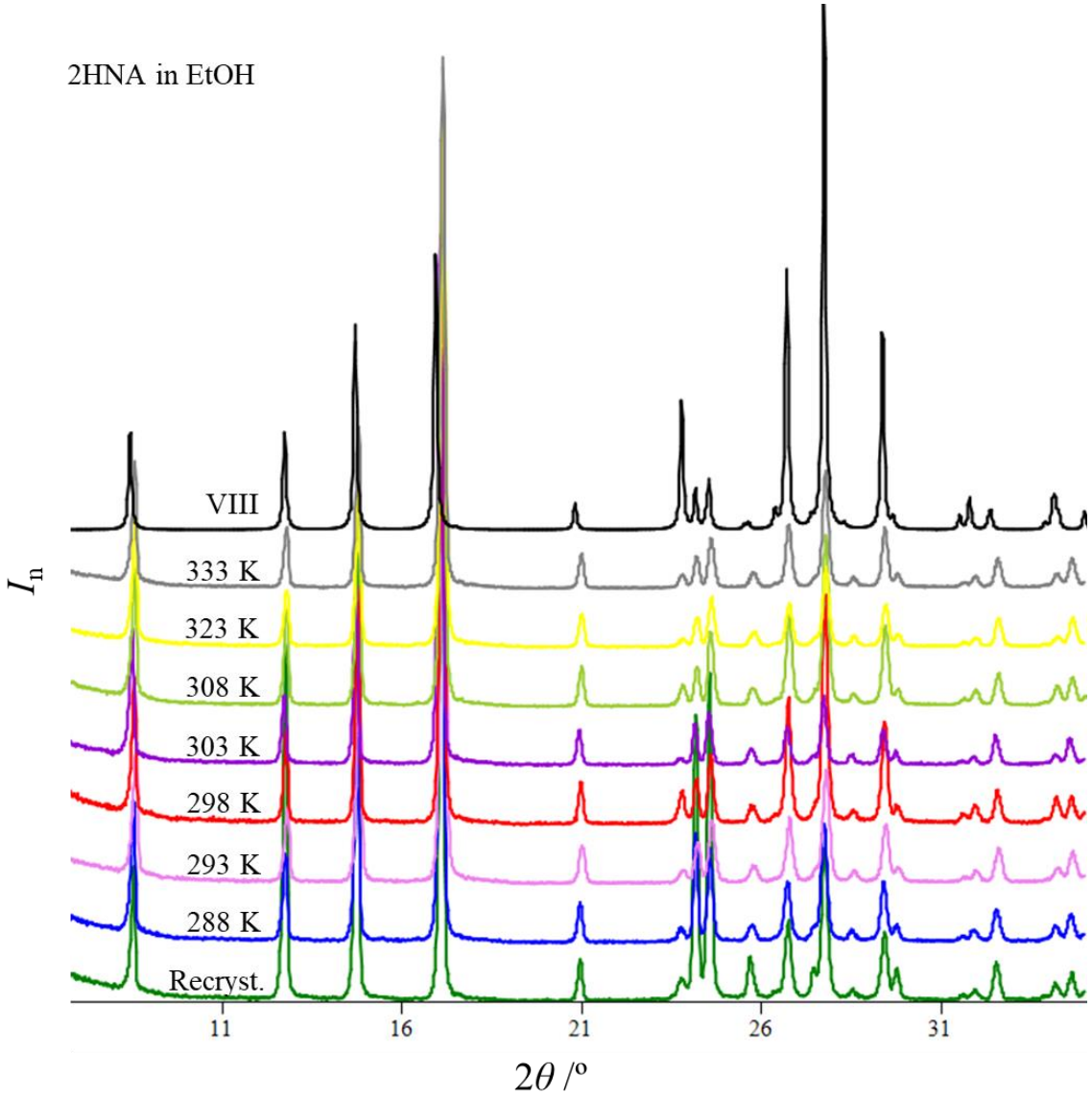

Fig. S24. Comparison of X-ray diffraction patterns obtained at room temperature for the recrystallized 2HNA (bottom), the powders obtained during the solubility experiment performed in EtOH (middle patterns matching form VIII, the stabilization temperatures used in the slurry are specified), and the pattern from the literature matching structure [3] (top). All the diffractograms were normalized to the peak of highest intensity (I_n) and plotted using EasyGraphII [1].

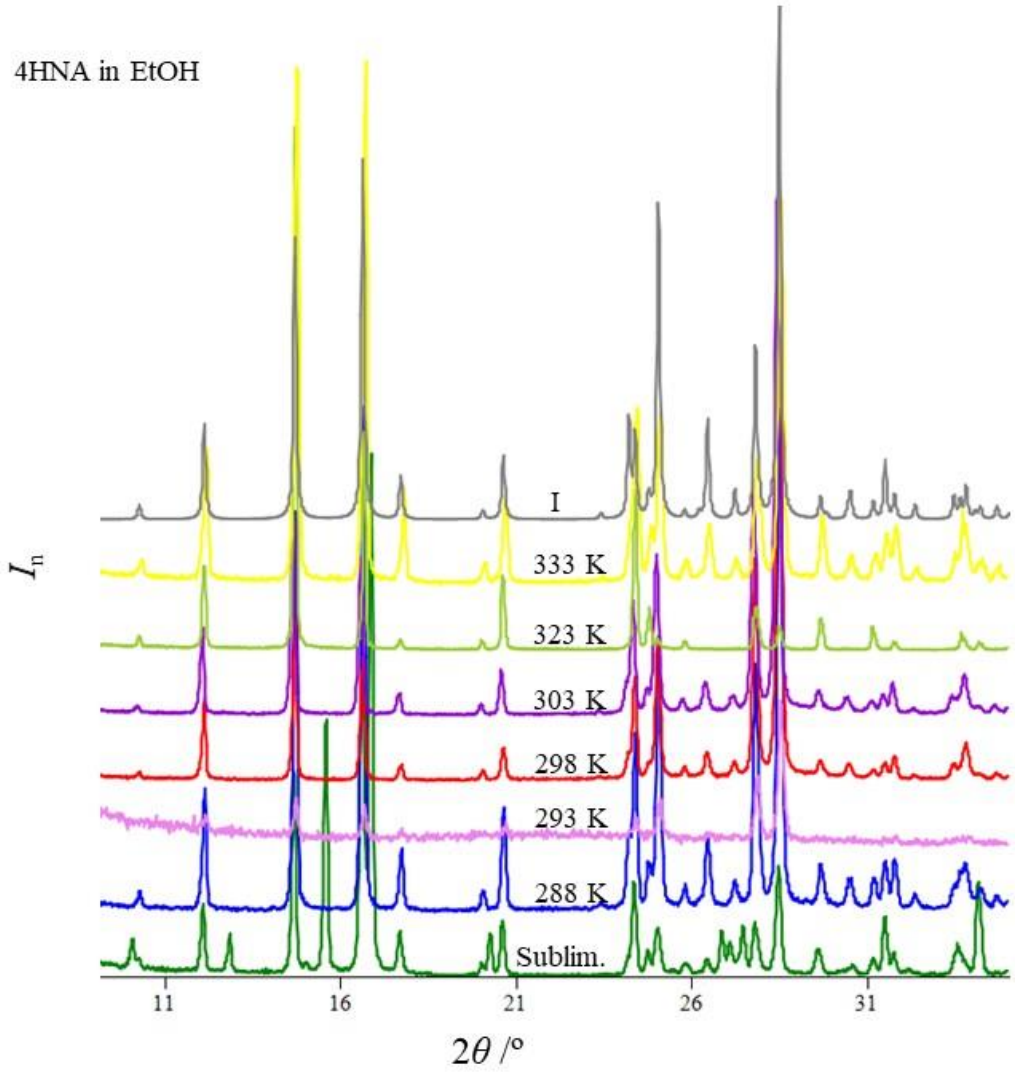

Fig. S25. Comparison of X-ray diffraction patterns obtained at room temperature for the sublimed 4HNA (bottom), the powders obtained during the solubility experiment performed in EtOH (middle patterns matching form I, the stabilization temperatures used in the slurry are specified), and the pattern from the literature matching structure [3] (top). All the diffractograms were normalized to the peak of highest intensity (I_n) and plotted using EasyGraphII [1].

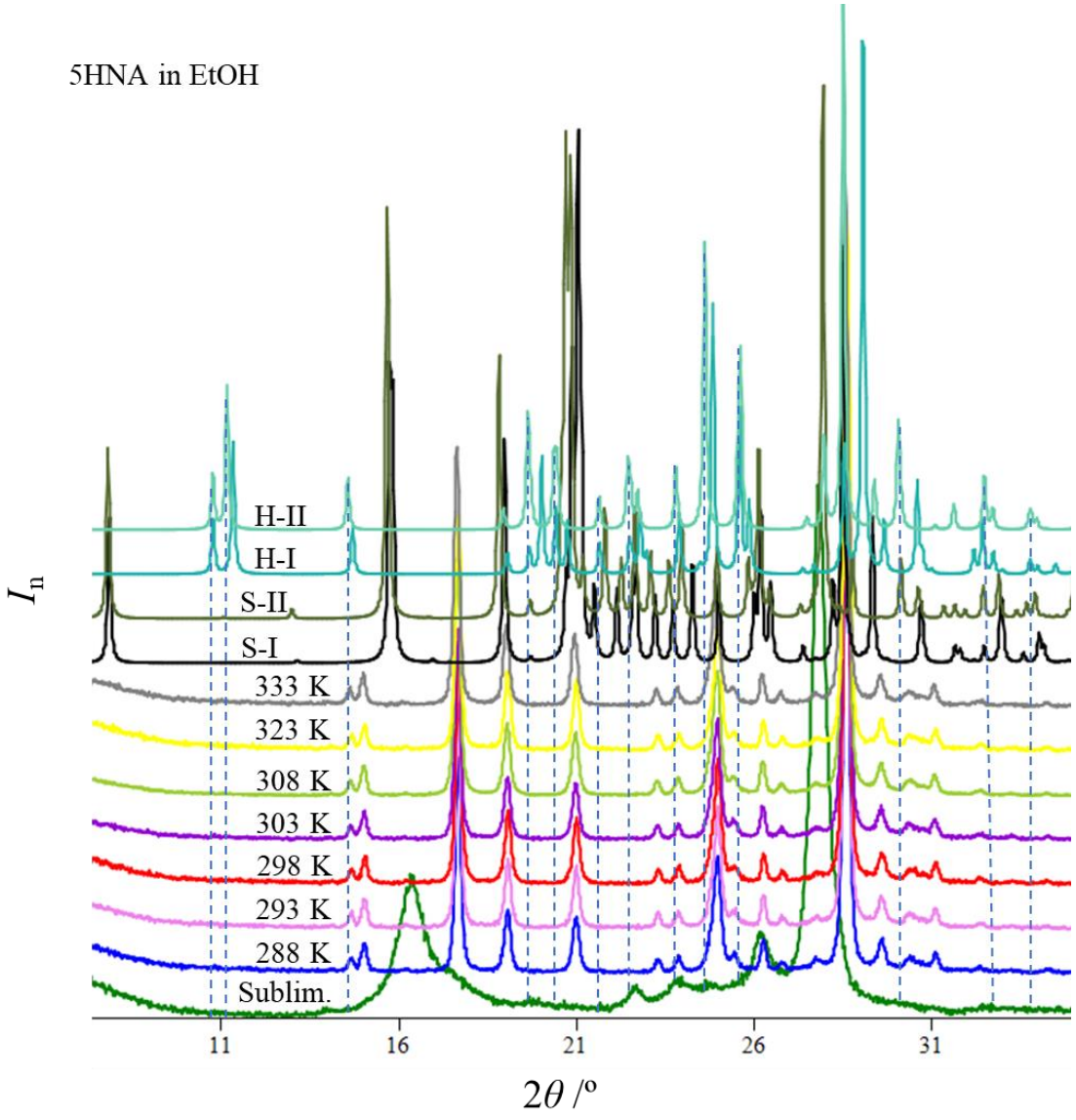

Fig. S26. Comparison of X-ray diffraction patterns obtained at room temperature for the sublimed 5HNA (bottom), the powders obtained during the solubility experiment performed in EtOH (middle patterns, the stabilization temperatures used in the slurry are specified), and the patterns from the hydrate and DMSO-solvate structures from our group already in the literature [2] (top). All the diffractograms were normalized to the peak of highest intensity (I_n) and plotted using EasyGraphII [1].

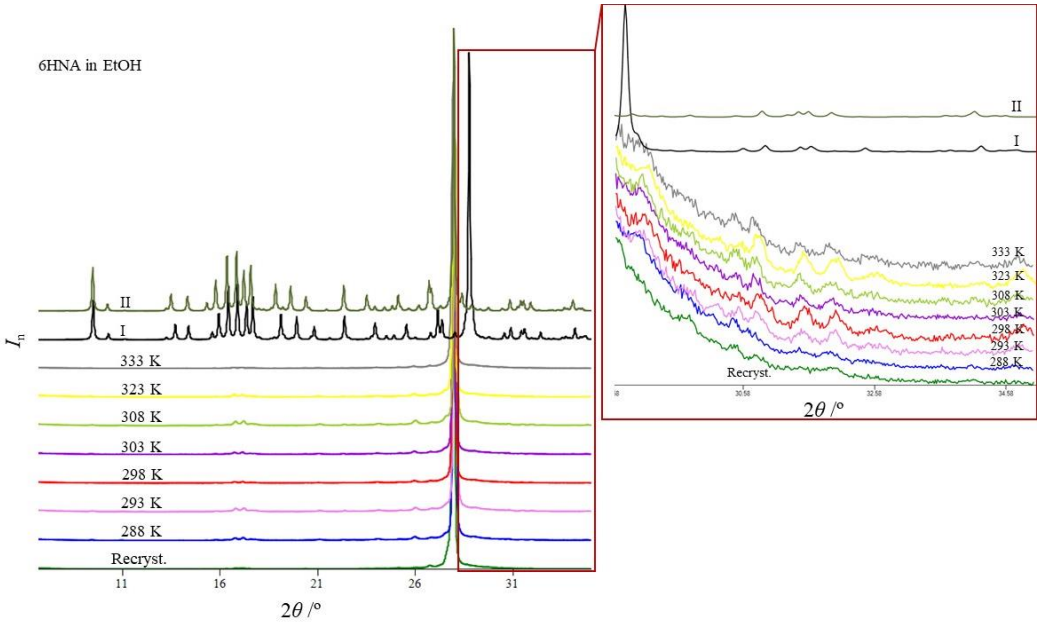

Fig. S27. Comparison of X-ray diffraction patterns obtained at room temperature for the recrystallized 6HNA (bottom), the powders obtained during the solubility experiment performed in EtOH (middle patterns matching form II, the stabilization temperatures used in the slurry are specified), and the patterns from the literature polymorph structures (top, for references see Table 1). A zoom was added focusing on the region above the observed preferential orientation (2θ = 28.0) to ensure that at 2θ = 28.8 no peak was found, corroborating that the patterns obtained were in form II. All the diffractograms were normalized to the peak of highest intensity (I_n) and plotted using EasyGraphII [1].

Table S2

Indexation of the X-Ray Powder Diffraction Pattern of 2HNA·H_2O Recorded at 295±2 K, in the Range $7^o \leq 2\theta \leq 35^o$; Space Group $P2_1/n$; a = 3.810(1) Å, b = 7.370(2) Å, c = 20.749(6) Å, β = 89.96(9).

h	*k*	*l*	2*θ*(Obs)/º	2*θ*(Calc)/º
0	0	2	8.520	8.524
0	1	1	12.755	12.747
0	1	2	14.740	14.745
0	0	4	17.095	17.095
0	1	4	20.950	20.943
-1	0	1	23.755	23.746
0	2	0	24.165	24.153
0	2	1	24.530	24.537
0	2	2	25.665	25.656
-1	0	3	26.720	26.721
0	2	3	27.445	27.426
1	1	2	27.710	27.720
0	1	6	28.505	28.513
-1	1	3	29.385	29.388
0	2	4	29.750	29.741
1	0	5	31.880	31.875
0	2	5	32.450	32.496
0	1	7	32.545	32.562
1	1	5	34.175	34.176
0	0	8	34.615	34.586

Table S3

Indexation of the X-Ray Powder Diffraction Pattern of 6HNA Recorded at 295±2 K, in the Range $7^o \leq 2\theta \leq 35^o$; Space Group *P*-1; a = 6.9975(1) Å, b = 11.2333(2) Å, c = 16.2909(4) Å, β = 78.36(2).

h	*k*	*l*	2*θ*(Obs)/º	2*θ*(Calc)/º
0	1	1	9.420	9.476
1	0	1	13.440	13.457
-1	0	1	15.305	15.277
0	-2	0	16.370	16.352
0	2	1	16.855	16.827
1	-1	0	17.115	17.145
1	-1	1	17.530	17.514
-1	-2	1	20.370	20.424
-1	-1	3	24.055	24.043
1	3	0	25.180	25.155
-1	-3	1	26.735	26.743
2	2	0	27.975	27.964
0	3	3	28.685	28.693
1	2	5	30.455	30.451

Table S4

Microscopy images and SEM images of the HNA starting materials used in this work.

Sample		
2HNA recrystallized from water	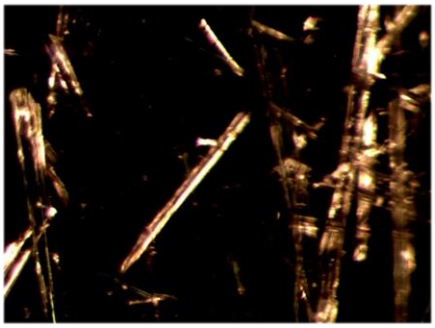	
	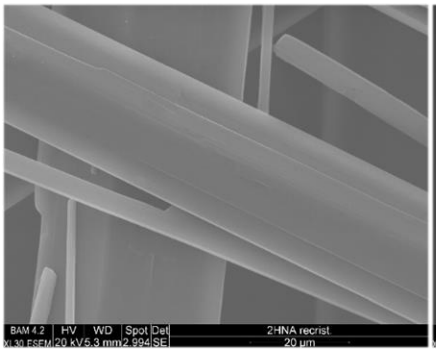	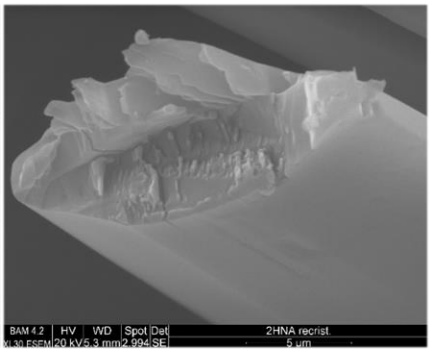
4HNA sublimed	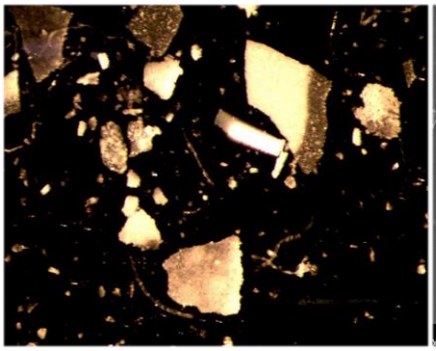	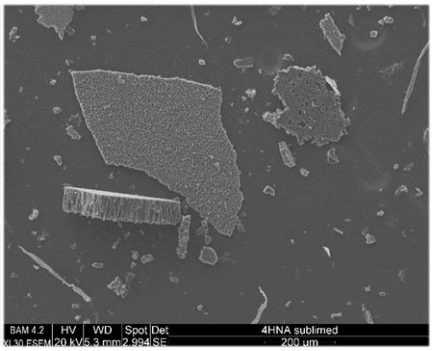
	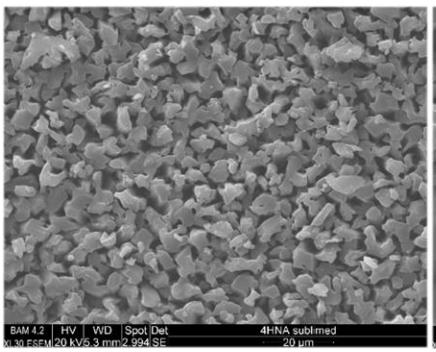	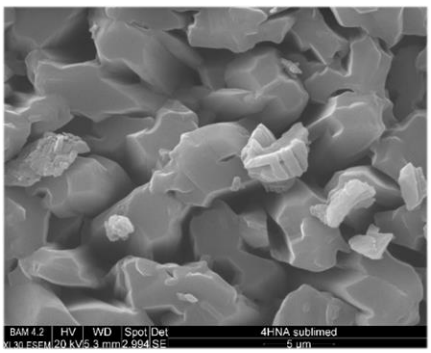

5HNA sublimed

6HNA recrystallized from water

Table S5

Temperature dependency of the mole fraction (x_{HNA}) equilibrium solubilities of HNAs[a]

	H_2O		EtOH	
	T/K	$10^3 \cdot x$	*T*/K	$10^3 \cdot x$
2HNA	288.77	0.180±0.002(4)	285.57	0.670±0.074(4)
	293.81	0.230±0.006(4)	288.50	0.660±0.037(4)
	298.67	0.300±0.004(4)	295.20	0.840±0.038(4)
	308.68	0.440±0.010(4)	300.19	0.950±0.046(4)
	313.55	0.530±0.002(4)	303.49	1.280±0.026(4)
	318.70	0.670±0.002(4)	308.17	1.480±0.063(4)
	324.00	0.800±0.012(4)	313.49	1.650±0.017(4)
			318.42	1.860±0.018(4)
			323.48	1.940±0.023(4)
			333.17	2.430±0.100(3)
4HNA	287.07	0.900±0.008(4)	288.55	0.690±0.045(4)
	290.56	0.960±0.042(4)	300.08	0.940±0.015(4)
	293.81	1.120±0.009(3)	303.46	1.280±0.038(4)
	298.49	1.370±0.010(3)	308.02	1.390±0.056(4)
	303.34	1.560±0.009(3)	313.29	1.670±0.026(4)
	312.57	2.520±0.137(3)	318.24	0.730±0.011(4)
	317.17	2.910±0.159(3)	323.24	2.220±0.043(4)
	322.54	3.400±0.190(3)	328.14	2.780±0.093(4)
5HNA	289.10	0.110±0.003(4)	285.65	0.470±0.218(3)
	293.87	0.130±0.002(4)	290.64	0.620±0.023(4)
	298.71	0.150±0.002(4)	295.29	0.630±0.026(4)
	303.70	0.170±0.004(4)	300.08	0.920±0.009(5)
	309.25	0.210±0.003(4)	303.47	0.940±0.030(4)
	313.61	0.245±0.004(4)	307.42	1.080±0.031(4)
	319.00	0.280±0.001(4)	318.12	1.510±0.036(4)
	323.86	0.320±0.002(4)	323.19	1.470±0.016(4)
	327.81	0.360±0.005(4)	327.98	0.740±0.199(3)
	333.59	0.430±0.002(4)		
6HNA	288.83	0.090±0.004(5)	285.78	0.390±0.005(5)
	293.74	0.110±0.002(4)	288.65	0.410±0.055(4)
	298.52	0.140±0.003(4)	295.31	0.510±0.095(4)
	303.38	0.180±0.003(4)	300.08	0.530±0.036(4)
	308.35	0.210±0.008(4)	303.45	0.660±0.052(4)
	318.29	0.260±0.004(4)	308.35	0.770±0.077(4)
	322.93	0.290±0.002(4)	313.32	0.890±0.036(4)
	327.61	0.350±0.005(4)	317.97	0.990±0.023(4)
	333.25	0.440±0.001(4)	323.04	1.010±0.068(4)
			327.87	1.330±0.020(4)
			332.48	1.370±0.092(4)

[a] The indicated uncertainties in parenthesis relate to twice the standard error of the mean of the number of experiments.

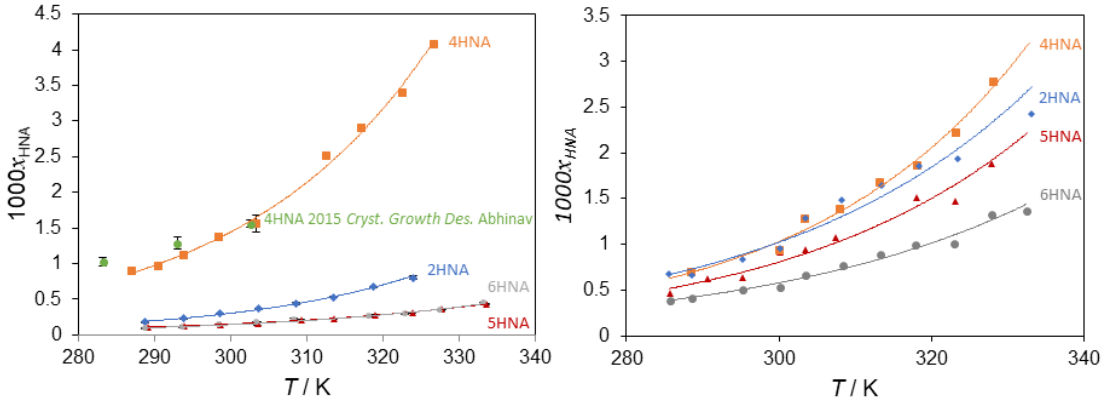

Fig. S28. Left: mole fraction solubilities ($1000x_{HNA}$) versus T plot obtained in this work for water (data for 4HNA in water from reference [4] is also represented); right: and a similar plot attained for ethanol.

Table S6. Hydroxynicotinic and nicotinic acids polymorphs

HNA	Form	Polymorph	Crystal system	Space group	a /Å	b /Å	c /Å	α /°	β /°	γ /°	*T*/K	Crystallisation solvents	Ref.
2	oxo	I	monoclinic	$P2_1/n$	3.640	11.584	13.565	90	94.64	90	90	H_2O	[5]
	oxo	V	monoclinic	$P2_1/n$	3.7473	7.3660	20.501	90	91.138	90	150	-	[6]
	oxo	VI	monoclinic	$P2_1/c$	3.7984	7.3494	20.3640	90	90.17	90	293	acidic solution (pH 1)	[7]
	oxo	VII	monoclinic	$P2_1/n$	3.8040	7.3640	20.741	90	90.01	90	293	EtOH	[8],[9]
	oxo	VIII	monoclinic	$P2_1/n$	3.797	7.354	20.905	90	90.007	90	293	H_2O	[3]
	oxo	I (= [5])	monoclinic	$P2_1/n$	3.640	11.584	13.565	90	94.64	90	90	MeOH+2-CNA+*p*-TsOH,MeOH+DCMA+*p*-TsOH,MeOH+HCl,EtOH+HCl,EtOAc+*p*-TsOH	[10]
	oxo	II	monoclinic	$P2_1/n$	3.725	7.368	20.417	90	91.47	90	90	MeOH,EtOH,H_2O,*i*-PrOH,AcO,DMSO,EtOAc,DMF,AcOH,MeOH+2-CNA,MeOH+DCMA	[10]
	oxo	III	monoclinic	$P2_1/c$	9.997	3.754	15.362	90	106.31	90	90	H_2O+*p*-TsOH	[10]
	oxo	IV	monoclinic	$P2_1/c$	9.773	4.0520	14.993	90	109.95	90	90	MeOH+*p*-TsOH, EtOH+*p*-TsOH, H_2O+*p*-TsOH	[10]
4	oxo	H-I	orthorhombic	$P2_12_12$	7.227	23.701	3.6999	90	90	90	296	1:2 (v/v) EtOH/H_2O	[11]
	oxo	I	monoclinic	$P2_1/c$	3.804	14.582	10.673	90	94.254	90	293	EtOH	[3]
	oxo	II	orthorhombic	$Pna2_1$	13.4233	3.8097	11.6150	90	90	90	90	MeOH	[12]
	oxo	III	monoclinic	$P2_1/c$	3.7198	14.5367	10.6250	90	93.3280	90	90	AcO, EtOAc, *i*-PrOH	[12]
	hydroxy	IV	monoclinic	Cc	3.6124	22.8112	13.5495	90	89.8980	90	90	EtOH	[12]
	hydroxy	H-II	orthorhombic	$P2_12_12$	7.2840	23.5200	3.6450	90	90	90	90	H_2O	[12]
	oxo	H-III	monoclinic	$P2_1/c$	7.8418	12.6104	7.2017	90	113.9211	90	90	H_2O	[12]
5	zwitt. 2	H-I	monoclinic	$P2_1/c$	4.504	16.389	8.856	90	91.271	90	167	H_2O	[2]

	zwitt.2	H-II	monoclinic	*P*2$_1$/*c*	4.4942	16.396	9.0283	90	89.977	90	296	H_2O	[2]
	hydroxy	S-I	monoclinic	*P*2$_1$/*c*	5.2351	22.4779	8.4174	90	94.301	90	167	DMSO	[2]
	hydroxy	S-II	monoclinic	*P*2$_1$/*c*	5.2638	22.580	8.5353	90	93.269	90	296	DMSO	[2]
6	oxo	I	triclinic	*P*-1	6.8130	11.1340	16.2780	82.5570	78.106	76.251	90	DMSO	[13]
	oxo	II	triclinic	*P*-1	6.976	11.231	16.290	82.553	78.279	75.166	293	H_2O	[3]
NA		I	monoclinic	P2$_1$/c	7.175(2)	11.682(2)	7.220(2)	90	113.38(5)	90	r.t.	_	[14]
		“	“	P2$_1$/c	7.162	11.703	7.242	90	113.2	90	r.t.	_	[15]
		“	“	P2$_1$/c	7.186(2)	11.688(3)	7.231(2)	90	113.55(6)	90	r.t.	_	[16]
		“	“	P2$_1$/c	7.303(11)	11.693(2)	7.33(3)	90	113.68(14)	90	r.t.	_	[17]
		“	“	P2$_1$/c	7.41(3)	11.692(2)	7.377(11)	90	114.45(14)	90	r.t.	_	[17]
		“	“	P2$_1$/c	7.1672(5)	11.6710(6)	7.1057(6)	90	114.785(10)	90	150	Oil droplets	[18]

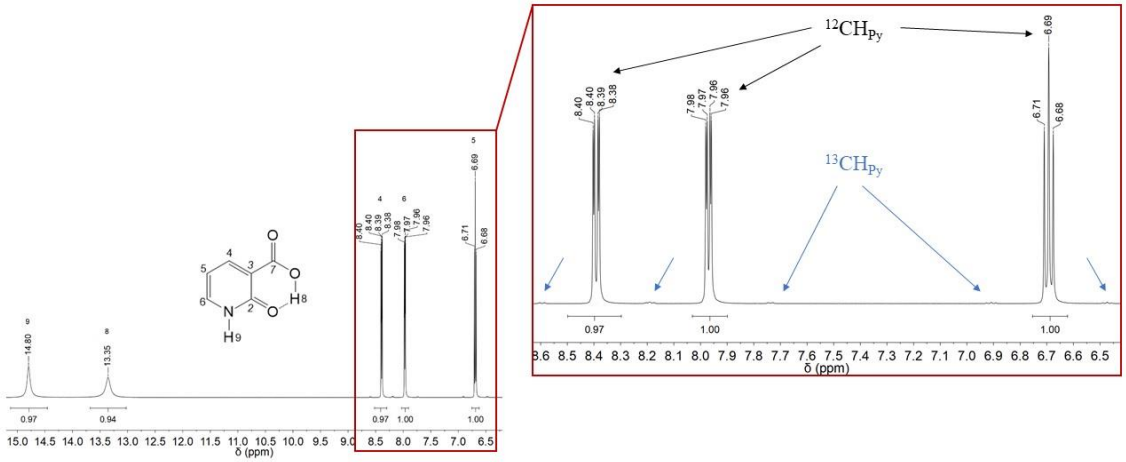

Fig. S29. ^{1}H NMR spectrum of 2HNA in DMSO-*d*$_6$ with a zoom detail for the coupling displayed by the $^{12}CH_{Py}$ resonances (please note that the satellite peaks present near the baseline are due to the $^{13}CH_{Py}$ which exist with the natural abundance of 1 %).

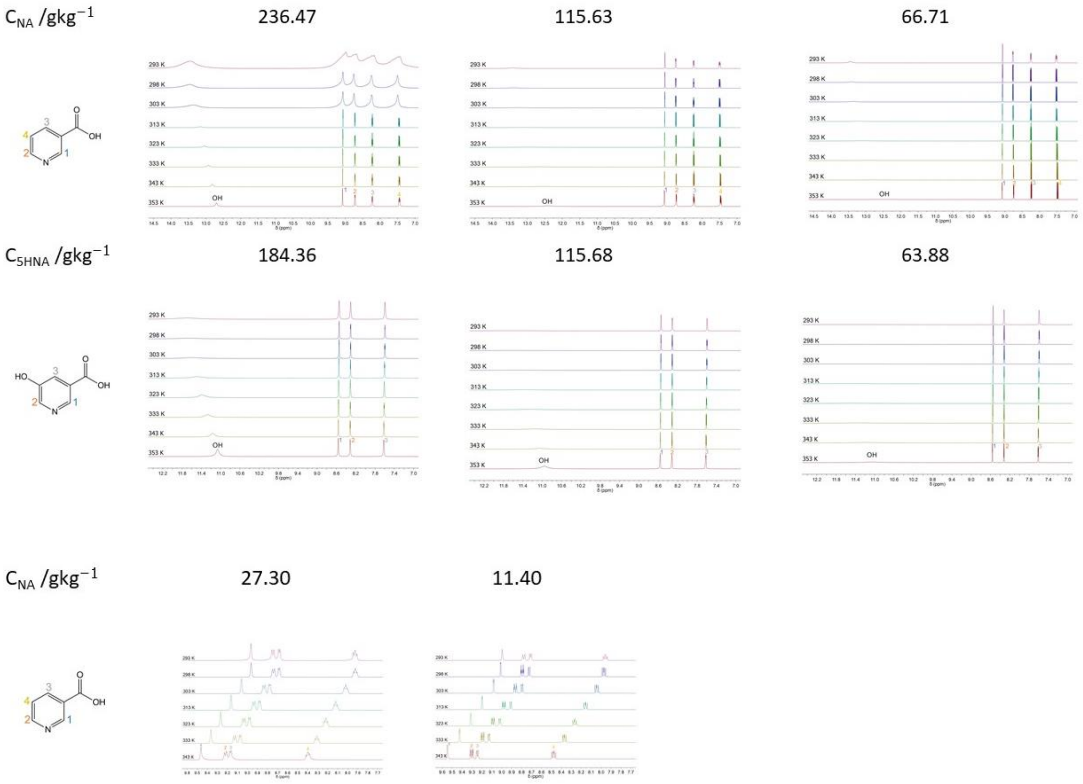

Fig. S30. ^{1}H-NMR spectra for the cooling crystallisation of nicotinic acid in DMSO-*d*$_6$ (top) and D_2O (bottom), and of 5-hydroxynicotinic acid in DMSO-*d*$_6$ (middle), at different concentrations.

References

[1] C.E.S. Bernardes, EASY GRAPH II. <https://webpages.ciencias.ulisboa.pt/~cebernardes/EasyGraph/Software-win-EG.html>, 2019.

[2] A. Joseph, J.S. Rodrigues Alves, C.E.S. Bernardes, M.F.M. Piedade, M.E. Minas da Piedade, Crystengcomm 21 (2019) 2220-2233.

[3] R.C. Santos, R.M. Figueira, M.F. Piedade, H.P. Diogo, M.E. Minas da Piedade, J. Phys. Chem. B 113 (2009) 14291-14309.

[4] A. Joseph, C.E.S. Bernardes, A.S. Viana, M.F.M. Piedade, M.E.M. da Piedade, Cryst. Growth. Des. 15 (2015) 3511-3524.

[5] S. Long, M. Siegler, T. Li, Acta Cryst. Sec. E 62 (2006) o5664-o5665.

[6] S. Djurdjevic, D. Leigh, S. Parsons, CCDC 660787: Experimental Crystal Structure Determination, 2008.

[7] B.-M. Kukovec, Z. Popović, G. Pavlović, M. Rajić Linarić, J. Mol. Struct. 882 (2008) 47-55.

[8] J. Miklovič, P. Segľa, D. Mikloš, J. Titiš, R. Herchel, M. Melník, (2010).

[9] J. Miklovič, P. Segľa, D. Mikloš, J. Titiš, R. Herchel, M. Melník, Chem. Papers 62 (2008).

[10] S.H. Long, P.P. Zhou, K.L. Theiss, M.A. Siegler, T.L. Li, Crystengcomm 17 (2015) 5195-5205.

[11] E.P. Matias, C.E.S. Bernardes, M.F.M. Piedade, M.E.M. da Piedade, Cryst. Growth. Des. 11 (2011) 2803-2810.

[12] S.H. Long, M.T. Zhang, P.P. Zhou, F.Q. Yu, S. Parkin, T.L. Li, Cryst. Growth. Des. 16 (2016) 2573-2580.

[13] S. Gupta, S. Long, T. Li, Acta Cryst. Sec. E 63 (2007) o2784-o2784.

[14] W.B. Wright, G.S.D. King, Acta Crystallographica 6 (1953) 305-317.

[15] M.P. Gupta, P. Kumar, Crystal Struct. Commun. (1975) 365.

[16] A. Kutoglu, C. Scheringer, Acta Crystallographica Section C Crystal Structure Communications 39 (1983) 232-234.

[17] E. van Genderen, M.T. Clabbers, P.P. Das, A. Stewart, I. Nederlof, K.C. Barentsen, Q. Portillo, N.S. Pannu, S. Nicolopoulos, T. Gruene, J.P. Abrahams, Acta Crystallogr A Found Adv 72 (2016) 236-242.

[18] A.R. Tyler, R. Ragbirsingh, C.J. McMonagle, P.G. Waddell, S.E. Heaps, J.W. Steed, P. Thaw, M.J. Hall, M.R. Probert, Chem 6 (2020) 1755-1765.